Taylor & Francis
Taylor & Francis Group

FULL PAPER

Realizing whole-body tactile interactions with a self-organizing, multi-modal artificial skin on a humanoid robot

P. Mittendorfer[a]*, E. Yoshida[b] and G. Cheng[a]

[a]*Institute for Cognitive Systems, Technische Universität München, Munich, Germany;* [b]*Joint Robotics Laboratory, CNRS-AIST, Tsukuba, Japan*

In this paper, we present a new approach to realize whole-body tactile interactions with a self-organizing, multi-modal artificial skin on a humanoid robot. We, therefore, equipped the whole upper body of the humanoid HRP-2 with various patches of CellulARSkin – a modular artificial skin. In order to automatically handle a potentially high number of tactile sensor cells and motors units, the robot uses open-loop exploration motions, and distributed accelerometers in the artificial skin cells, to acquire its self-centered sensory-motor knowledge. This body self-knowledge is then utilized to transfer multi-modal tactile stimulations into reactive body motions. Tactile events provide feedback on changes of contact on the whole-body surface. We demonstrate the feasibility of our approach on a humanoid, here HRP-2, grasping large and unknown objects only via tactile feedback. Kinesthetically taught grasping trajectories, are reactively adapted to the size and stiffness of different test objects. Our paper contributes the first realization of a self-organizing tactile sensor-behavior mapping on a full-sized humanoid robot, enabling a position controlled robot to compliantly handle objects.

Keywords: artificial skin; self-organization; whole-body tactile interaction; humanoid robots

1. Introduction

1.1. Motivation

Human naturally handles whole-body contacts during everyday life – e.g. manipulating large objects with the whole body. Robots instead are commonly limited to manipulations with their end effectors. Besides cognitive capabilities, robots lack a primary sense for handling those close encounters ? whole-body tactile sensing. Compensating the lack of artificial skin with other senses is hardly possible. Vision cannot directly measure force, suffers from occlusion and a lack of precision for fine manipulation. With joint-level force sensing, it is difficult to differentiate internal from external forces and difficult/impossible to resolve multiple simultaneous contact points or collinear forces. Sensitive skin instead, can provide a rich and direct feedback, from numerous simultaneous contact points and a large area of contact. Sensitive skin is thus a key component to bring robots into contact rich everyday life – be it as work companion or service robot. Due to a magnitude of challenges, deploying and effectively utilizing a high number of tactile sensors, on large and arbitrary 3D surfaces, whole-body tactile sensing is not yet solved.

1.2. Related works

Detailed requirements for tactile sensing date back to the early 1980s,[1] but today's robots still lack the effective utilization of tactile skin.[2] Artificial skin is not just a high density sensor matrix,[3] but a highly distributed sensor system.[4] Systematic aspects like distributed computing, sensor [5] and power wiring,[6] robustness,[7] and manufacturability have to be taken into account.[4] A long-term desire is the so called system on a chip,[8] but costs and complexity are so far limiting a breakthrough in this area. Existing full-body skins are only modular at the level of individual patches of skin,[9–12] giving way of some of the flexibility. Before utilization, artificial skin has to be spatially calibrated.[13] Manually calibrating a growing number of distributed sensors on a large and arbitrarily shaped surface is error prone and cumbersome. Robots should utilize their own sensors and action capabilities to build their body knowledge.[14] The strongly linked kinematic calibration is heavily biased towards manipulator arms observed by a camera [15] – a solution that is not viable for optically in-discriminable skin. Tactile point probing approaches are limited by the reachability of the robot and commonly shown in simulation only.[16] A real world implementation in [17], requires a fully calibrated force/torque sensor at the shoulder and 'tedious' manual probing. Although accurate explicit models would be optimal for standard control approaches,[15] coarse implicit models seem a good alternative to represent the own body [18] and to enable sensory guided motor control.[19] Common tactile control schemes are optimized towards certain tasks

---

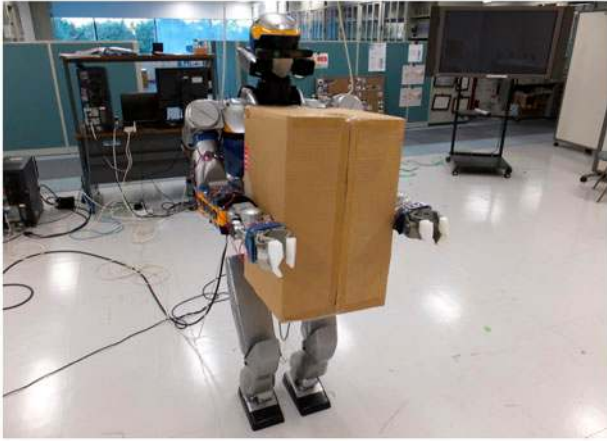*Corresponding author. Email: philipp.mittendorfer@tum.de

Figure 1. A non-compliant robot (HRP-2) holding a large and unknown object, adaptively grasped via tactile feedback and a self-explored body knowledge.

– e.g. to follow contact trajectories [20] or to trigger motion primitives.[21] Only few groups managed to bring whole-body tactile sensing to the application level. In [22,23], tactile sensors are utilized to control the contact between a human-like object and the arms of a nursing robot. The approach is currently limited to fine manipulation around an initial contact state. In [24], tactile feedback and additional contact points enable a humanoid to lift heavy objects and in [25] a multi-axis soft tactile sensor suit is utilized to detect contact states for receiving and releasing objects from and to human. Alas, both papers are not very precise on the haptic control strategy – we estimate tactile feedback solely serves to switch between pre-computed procedures.

In parts, this paper is also based on our own previous works. We utilized the second version of our tactile modules,[26] first introduced in [27]. The self-acquired kinematic knowledge in this paper is based on our kinematic tree algorithm explained in [28] and our postural sensory-motor mapping, first introduced in [29]. Our work on grasping large, unknown objects with HRP-2 [30] and the Stack of Tasks,[31] has been previously published in [32].

1.3. Contribution

This paper introduces a systematic approach to realize whole-body tactile sensing on robots. Our main contributions are: (a) the development of a scalable, multi-modal, modular artificial sensor skin network; (b) algorithms to automatically self-organize large area deployments of the skin on robots with numerous revolute joints; (c) the development of a reactive and event driven control framework to monitor and react on distributed, multi-modal tactile stimulations; (d) the effective utilization of tactile kinesthetic teaching for whole-body human robot interaction; and (e) the realization of an exemplary whole-body, close-contact tactile grasping task. Due to the versatility of our system,

and its plug&play capabilities, we can effortlessly enhance non-compliant robots with compliance. We made use of a biped to demonstrate the feasibility of our self-organization approach – even with dynamic perturbations on an inertial frame. The chest and arms of the humanoid enabled whole-body interactions (see Figure 1).

2. Creating whole-body artificial skin

The design of artificial skin from the same intelligent cell (see Figure 2) has many advantages. Amongst others, a cellular skin is easily scalable and transferable between robots and applications.

2.1. Cell design

2.1.1. Shape

Only three uniform shapes can tessellate a plane without gaps: triangles, rhomboids, and hexagons. We consider the hexagonal shape optimal. The hexagon allows to establish physical data and power connections between all neighbors. The distance of the sensors between neighboring hexagons is equal. Its close to circular density offers space for large components, while evenly distributing deformation stress, especially with flex-rigid solutions.

2.1.2. Flexibility

In order to conform to arbitrary 3D surfaces, artificial skin must be flexible. We utilize rigid elements, but introduce bend-ability and stretchability at the flexible interconnections between those elements. In this way, we can apply standard rigid electronics as well as future flexible electronics. Reducing the size of the rigid elements increases the amount of interconnections and such the flexibility.

2.1.3. Sensors

With multiple sensor modalities, we emulate human cues of touch (refer to Table 1). Human skin can sense the lightest touch, we emulate this cue with a proximity sensor. The advantage of having a sense of pre-touch with robots is the ability to react before making contact (e.g. to avoid impacts). We currently utilize an active optical proximity sensor, measuring the amount of reflected infrared light. Vibrational cues enable human to discriminate surface properties and detect impacts. With a 3-axis accelerometer, we can measure vibrations, motion acceleration, and the orientation towards gravity. The largest benefit of a tri-axial accelerometer in each skin cell, is the ability to quickly and automatically acquire body (e.g. kinematic) knowledge with open-loop motions of the robot. Temperature sensing plays an important regulatory role with human, but also contributes with artificial skin. Mechanical sensors must be compensated for thermal effects – e.g. when placed close
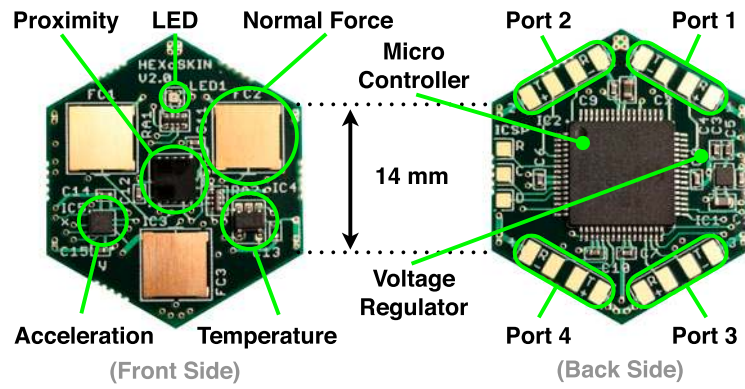
Figure 2. Electronics board of the modular artificial skin cell, featuring multiple sensor modalities on the front side, and local infrastructure on the back side.

Table 1. Multi-modal sensor specifications.

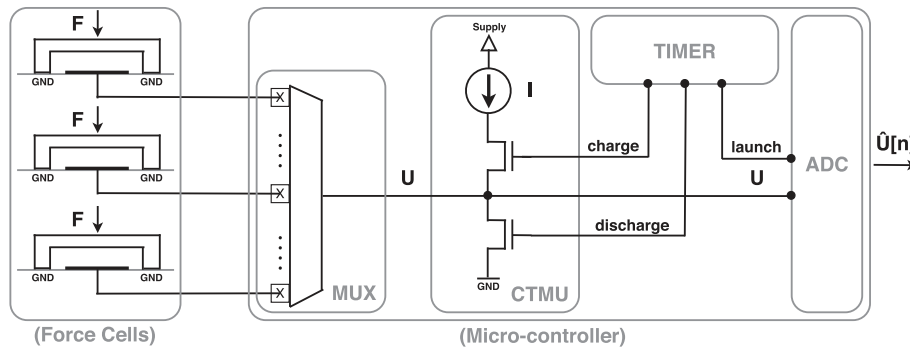| Modality	Pre-touch	Acceleration	Temperature	Normal force
Sensor	VCNL4010	BMA250	LM71	Custom
Size in mm	$4.0 \times 4.0 \times 0.8$	$2.0 \times 2.0 \times 1.0$	$3.0 \times 3.0 \times 1.0$	$6.0 \times 6.0 \times 0.1$
Resolution	16 bit	10 bit	14 bit	12 bit
Range	1–200 mm	$\pm 2/8/16$ g	-40 to 150 °C	>0–10 N
Bandwidth	0–250 Hz	0–1 kHz	0–7 Hz	0–33 kHz
Per cell	1	1	1	3
Power	3.8 mA	0.2 mA	0.7 mA	MC internals

Figure 3. Minimalistic electronics for all normal force sensors on the same sensor cell, fully built into the PIC24F micro controller.
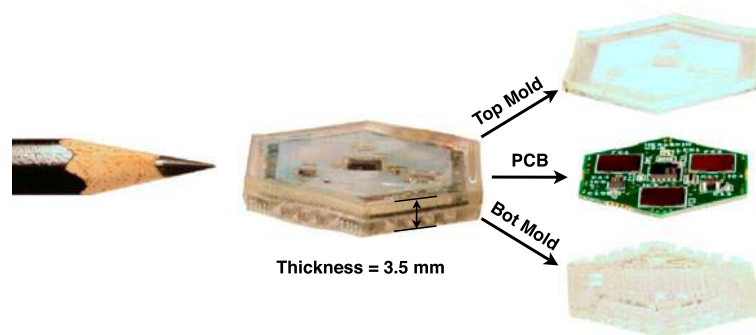

Figure 4. Skin layers of the sensor cell: top cover, electronics board and bottom cover.
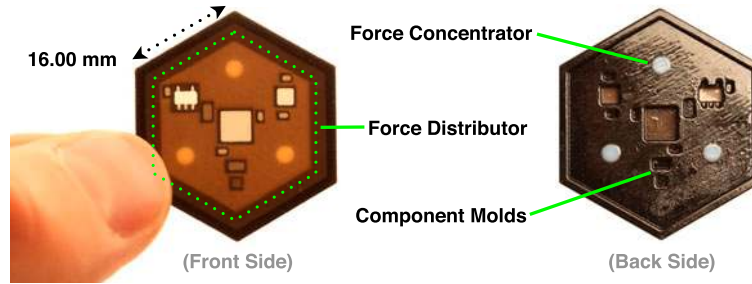
Figure 5. Micro-structured top cover of the sensor cell, with a micro-structure of soft and hard materials, to collect and concentrate distributed forces onto the discrete force sensors.

to active joints that can easily reach 70 °C on heavy duty. The temperature difference of the environment itself can be utilized to detect tactile properties – e.g. sense wind chill effects [27] or classify materials via thermal transfer rates. Artificial skin must be able to quantify the amount of force in order to control it. Due to a lack of available solutions, we developed a new normal force sensor, based on a circular metallic spring.[26] The displacement of the spring is measured capacitively, with electronics built into the local micro-controller (see Figure 3). Due to the metal spring, our sensor shows an almost linear thermal dependency, high dynamics, low hysteresis, and outstanding robustness. All sensors are promoted and protected by the three-dimensional structured material stack (see Figures 4 and 5), emulating the functional layers of human skin (e.g. focusing and filtering spatial stimuli).

2.1.4. Local processing

Parts of the signal processing algorithms, like low-pass filtering or thresholding, can already be performed locally. This decreases the repetition frequency and/or length of packets and thus reduces the network and high-level processing load. Digital signal transmissions also largely increase signal integrity in noisy environments, like on robots. Therefore, each cell can locally convert analog to digital signals, pre-process the digital signals, packet the conversion results, and route packets from cell-2-cell. Local memory is used to permanently store sensor calibration values, e.g. offsets, local settings, and the automatically distributed unique cell identifier (ID).

2.2. Cellular network

2.2.1. Cell-2-cell connection

In order to minimize the wiring effort, we developed a pattern with four non-crossing wires to bidirectionally transfer data and power between hexagon cells (see Figure 6). Power is routed passively through the resulting resistor ladder, with local voltage regulators to compensate the voltage drop and reduce power noise. With an active data routing scheme,
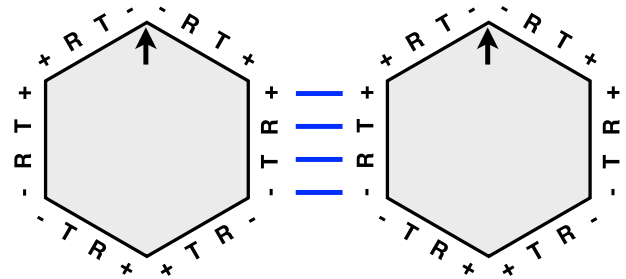

Figure 6. Port pattern for a direct cell-2-cell connection – (R)eception, (T)ransmission, (+) and (−) Power.

failures can be isolated – yielding robustness, while minimizing wirings. Since sensor cells behave like network repeaters, the signal does not loose strength and minimalistic transistor-2-transistor logic levels can be utilized. In a dense cell-2-cell network, adjacencies can also be inferred to real world distances, allowing a quick generation of topological maps.

2.2.2. Network self-organization

In order to efficiently handle a large and arbitrary networks, the skin system must automatically organize. Our network self-organization (see Figure 7) splits into four phases: First, we initiate a search for active connections. Next, we enforce directed communication trees with a sink at each interface port. This tree structure is then utilized to distribute unique IDs to all sensor cells. Finally, network adjacencies are acquired and forwarded to the control system. Redundancy allows to handle connection failures with a simple network re-organization, keeping the unique cell IDs in local memory in order to not to lose spatial calibration.

2.2.3. Interfacing and latency

Interfacing a smart cellular skin is user-friendly – every free port of a skin patch can be utilized to feed power and communication to the network (refer to Table 2). Additional interface connections improve redundancy, increase communication bandwidth, reduce latency, and strengthen the

Table 2. Cellular network specifications.

| Cell input voltage	3.0–5.5 V	Max cell power	≤16 mA/3.0 V
Weight per cell	≤ 3.0 g	Skin thickness	3.3 mm
Cell surface	665 mm^2	Elastic gap	4.0 mm
Number of interfaces	Unlimited	Number of cells	Unlimited
Cell2cell bandwidth	4 Mbit/s	Interface bandwidth	1 Gbit/s
Cell2cell protocol	Custom	Interface protocol	UDP
Cell2cell packets	20 bytes	Ports per cell	4
Packet routing	Round robin	Power routing	Resistive
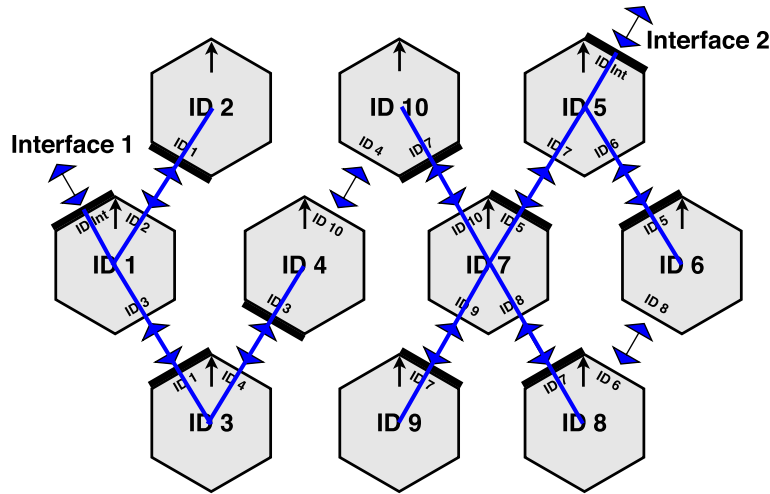
Figure 7. Example of the network organization – Detected active ports, set master ports, distributed IDs, and detected neighbors. Two boundary ports are connected to the interface.

power supply. On HRP-2, we utilized our Gigabit Ethernet FPGA interface with five ports, converting all cell packets to standard UDP and vice versa. The 688 ns time, to transfer a single-sensor cell data packet via UDP, is neglectable in comparison to routing delays within the sensor cell network. The worst-case forwarding delay, with a round robin scheduler on each cell, is currently 275 μs. For an update rate of 250 Hz, the depth of the communication tree should not be more than 14 units, while one interface port can theoretically handle up to 80 sensor cells.

3.   Deploying whole-body artificial skin on robots

3.1.   Integrating skin on robots

Integrating cellular artificial skin on robots is a cut&paste process onto the robot's surface, limited by the size, and flexibility of the basic skin element. Ideally, contact is supported by large deformable areas, which is why robots should feature smooth and deformable surfaces. Sharp and rigid edges instead, attract undesirable point contacts and prevent the grounding of contacts on the sensitive skin. Surface compliance would also improve safety on close interaction [33] and loosen control rate constraints. Otherwise forces on a rigid robot, making contact with a rigid

object, would ramp up quickly, limiting manipulation speeds to undesirably slow values. Robot designers should also account for the wiring of artificial skin. Ideally, skin can be integrated locally into the robotic backbone – e.g. connecting it to the motor controllers. This way communication delays could be lowered and reaction speeds (e.g. safety stops) enhanced. If this is not possible, a few wire channels between body parts should be reserved for skin. On HRP-2, UR-5, and the KUKA LWR arm, we had to run cables on the outside of the robot, making them prone to be ripped off, and to interfere with the robot motion and tactile sensation. With HRP-2, we placed our interface on the back of the robot, and connected it to the second on board computer (i686, 1.6 GHz, 2 cores, 3 MB L2, 32 GB RAM, Ubuntu 10.04) and on board power.

3.2.   Interfacing the control system

Our control approach is independent of a specific robot, but limited to common revolute degrees of freedom (DoFs). The requirements for the control interface are: (i) to publish the number of revolute degrees of freedom; (ii) to accept (emulated) velocity control values, and (iii) to give position feedback. In order to minimize control delays, we prefer an on board computer in order to locally process all tactile data.

$$^{u}\vec{a}_{u,d} = {}^{u}\underline{R}_w \cdot \left({}^{w}\vec{g} + {}^{w}\vec{a}_{u,d}^{tan} + {}^{w}\vec{a}_{u,d}^{cp} \right)$$
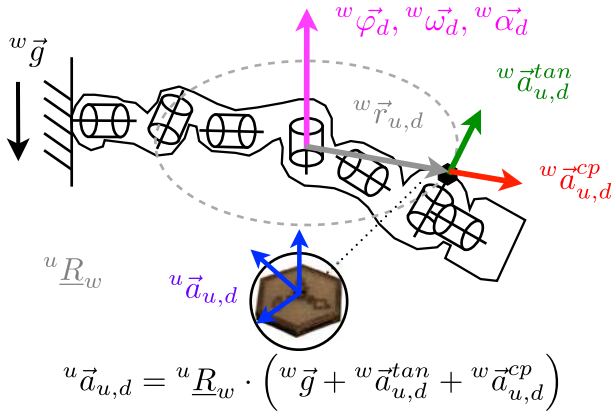
Figure 8. Components of the accelerometer reading, when actuating one revolute degree of freedom at a time.

The primary computer of HRP-2, for example, executes a 200 Hz control loop – the stack of tasks (SoT). The SoT controller generates actuator commands by resolving, in real-time, a set of prioritized tasks. In our experiments with HRP-2, equilibrium is achieved by fixing the feet and center of mass position to a static position. Redundancy then allows HRP-2 to realize whole-body manipulation while satisfying the equilibrium tasks. To generate grasping motions with the robot upper body, a low-priority task is added to the SoT, enforcing both arm velocities.

4. Automatically acquiring kinematic knowledge

4.1. *Using open-loop motion and distributed accelerometers*

Open-loop motions and distributed accelerometers are an efficient way to acquire (kinematic) body knowledge without time consuming, and potentially harmful, external or self-contacts. Small range open-loop motions can be quickly and safely executed, even on uncalibrated robots, while distributed accelerometers can, in parallel (for scalability), acquire information on the effects of those motions.

4.1.1. *Sensor actuator relations*

Here, we briefly describe the physical effects of an isolate revolute joint motion on accelerometers mounted on the actuated body parts (see Figure 8). Neglecting skin deformations, every sensor cell follows the acceleration of its mounting point. Given a single static reference body part (w), a change in velocity $\left(\frac{d}{dt}{}^{w}\omega_d(t) = {}^{w}\alpha_d(t) \right)$ of a revolute DoF (d) has a direct influence on the acceleration $^{u}\vec{a}_{u,d}$ of sensor cell (u), which superposes three different effects:

(a) The tangential acceleration $^{w}\vec{a}_{u,d}^{tan}$, which is dependent on the revolute acceleration $^{w}\vec{\alpha}_d$ and the radial vector $^{w}\vec{r}_{u,d}$, in between DoF (d) and

the accelerometer (u):

$$^{w}\vec{a}_{u,d}^{tan} = {}^{w}\vec{\alpha}_d \times {}^{w}\vec{r}_{u,d} \qquad (1)$$

(b) The centripetal acceleration $^{w}\vec{a}_{u,d}^{cp}$, which is dependent on the angular velocity $^{w}\vec{\omega}_d$ as well as the vector $^{w}\vec{r}_{u,d}$:

$$^{w}\vec{a}_{u,d}^{cp} = {}^{w}\vec{\omega}_d \times ({}^{w}\vec{\omega}_d \times {}^{w}\vec{r}_{u,d}) \qquad (2)$$

(c) And the gravity vector $^{w}\vec{g}$.

An accelerometer (u) senses all effects at the same time, in its local coordinate system:

$$^{u}\vec{a}_{u,d} = {}^{u}\mathbf{R}_w \cdot \left({}^{w}\vec{g} + {}^{w}\vec{a}_{u,d}^{tan} + {}^{w}\vec{a}_{u,d}^{cp} \right) \qquad (3)$$

The rotation matrix $^{u}\mathbf{R}_w$ in between the static reference frame and the accelerometer, as well as the vector $^{w}\vec{r}_{u,d}$, are dependent on the unknown kinematics of the robot. In this paper, we make use of the fact, that the tangential acceleration vector is co-linear with the motion vector.

4.1.2. *Constraints*

We assume joints with one or more revolute DoFs are connected by non-deformable body parts. During the whole calibration process, one reference body part has to remain static. With a robotic arm, this is naturally given by the base. For a humanoid robot, the torso is considered best, as it is a casual point to fix a humanoid, is located close to the center of mass and is a relatively central point in the kinematic tree. The static body part serves as root to the structural exploration and grounds all reactive motions. During exploration, it is necessary that every degree of freedom (DoF) can be actuated freely, without self- or environment collisions. Closed loops or under-actuated kinematics cannot be handled with our methods. The robot needs to be equipped with at least one sensor cell per body part, to fully explore its structure.

4.2. *Acquiring structural knowledge*

The structural self-exploration is an algorithm to automatically discover the robot's kinematic tree as a sequence of joints and body parts, carrying the skin. Structural knowledge is an important first step to build body knowledge – e.g. to assemble kinematic models or decouple body parts. The input to our structure extraction algorithm is the activity matrix.

4.2.1. *Activity matrix generation*

The activity matrix is a binary matrix with the following entries: (1) a '1' when a sensor cell is affected by the actuator; (2) a '0' when no motion or minor motion is detected (see Figure 9). In Section. 4.1.1 we summarized the effects we are able to measure with an accelerometer. Both dynamic
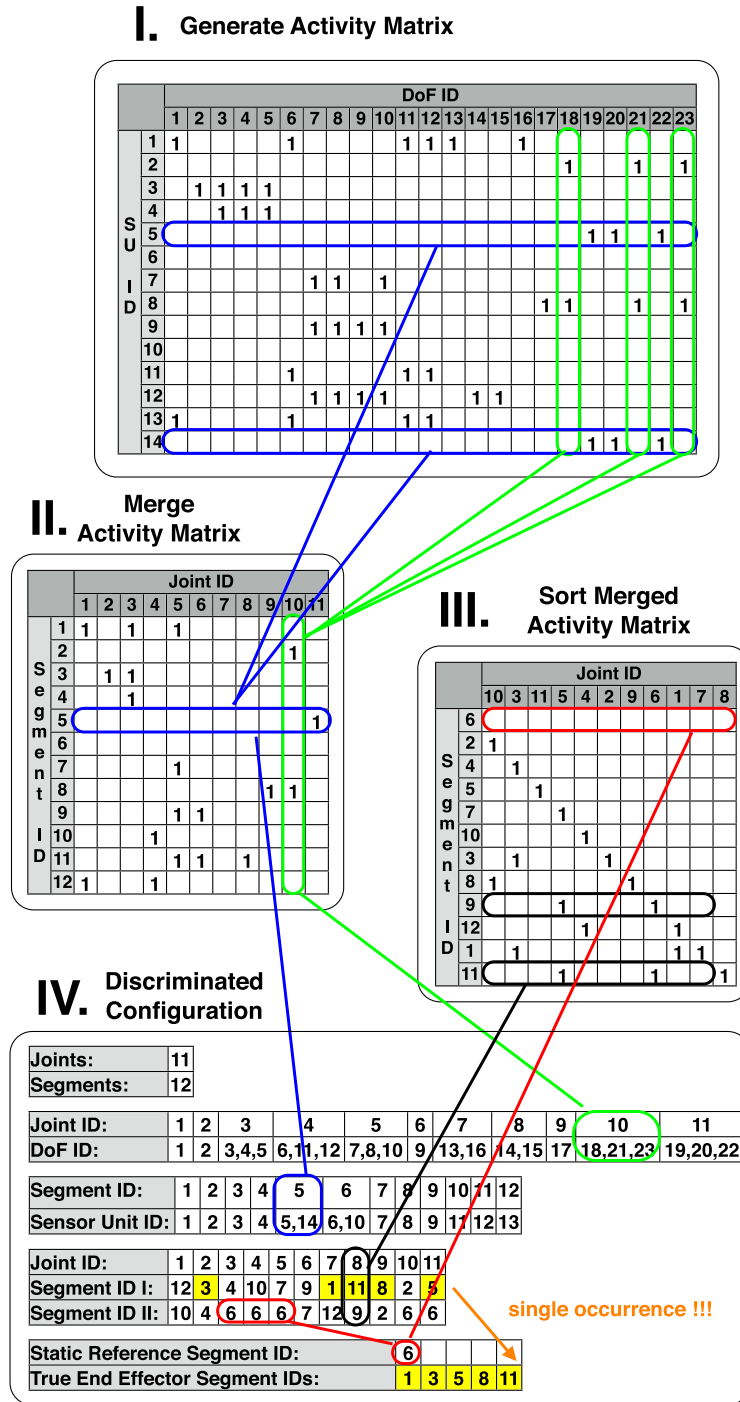
I. Generate Activity Matrix

II. Merge Activity Matrix

III. Sort Merged Activity Matrix

IV. Discriminated Configuration

Figure 9. Steps of the structure exploration algorithm for an activity matrix representing a 'simulated' humanoid robot (our test case).

effects vanish if the vector ($^{w}\vec{r}_{u,d}$) is close to zero. Rotating a DoF from one to another position, changes the orientation of all related body parts in the same way. Fixed thresholds can be applied to the static gravity vectors ($^{u}\vec{g}$) to detect if a rotation occurred. However, when a DoF axis is closely aligned to the gravity axis, the measured gravity vectors do not change and matrix entries are falsely set to '0'. To solve this problem, multiple activity matrices of the same robot can be combined with an element wise logical 'or'. A secure approach to generate two complementary activity matrices is to rotate the static segment of the robot around one of the horizontal axes e.g. a 'standing' and a 'lying' humanoid.

4.2.2. Segment and joint merging

Sensor cells that are located on the same body part encounter the same motion 'activity' and can be merged into body parts (see Figure 9). Similarly, all DoFs between body parts can be merged into joints. This leads to a merged activity matrix, correlating joint and body part activities (see Figure 9). The number of rows gives the number of detected body parts while the number of columns provides the number of joints. This is common for a tree like robotic structure, where the number of body parts (S) must be higher than the number of joints (J), i.e. $S = J + 1$.

4.2.3. Extracting connectivity

The merged activity matrix must be sortable to a strictly lower triangular form (see Figure 9). If this does not hold, one of the given constraints has been violated (refer to Section 4.1.2), e.g. there are body parts without skin cells. Our algorithm progresses along the secondary diagonal $(l_{(n+1)(n)}, n \in \mathbb{N})$, searching rows that are identical except for the current diagonal element, which is the joint that connects the two body parts (in Figure 9, we can observe that body parts 9 and 11 are connected by joint 8).

4.2.4. Kinematic tree

The extracted joint/body-part connectivity represents a hierarchical kinematic tree. The static reference body part (root) of the robot is the null row vector of the merged activity matrix. End effector body parts (leaves), like the finger tips of a humanoid, exactly connect to a single joint. Body parts that connect more than two joints, like the palm of a humanoid, are inner nodes and can serve as an intermediate reference for limbs. A limb is a kinematic chain, starting from a reference body part and ending at an end effector or inner node. With this information, we can hierarchically decouple the robot kinematic model, e.g. the two arms of a humanoid robot like HRP-2.

4.2.5. Experiment on HRP-2

We distributed ($U = 74$) sensor cells on the upper body of HRP-2, while having control on ($D = 14$) degrees of freedom of the left and right arm. All normalized gravity vectors $\vec{g}_{u,d,p}$ were measured in the initial pose (p) and final pose (f), when we change the position of a single DoF (d) one after the other with increments of $\varphi_\triangle = 0.1$rad. If the distance between both normalized vectors is above the pre-defined limit (lth), the corresponding entry ($am_{u,d}$) in the binary activity matrix (AM) is set to *true*:

$$am_{u,d} = \left| \frac{{}^u\vec{g}_{u,d}^p}{|{}^u\vec{g}_{u,d}^p|} - \frac{{}^u\vec{g}_{u,d}^f}{|{}^u\vec{g}_{u,d}^f|} \right| > l\text{th}, \quad am_{u,d} \in \{0, 1\} \tag{4}$$

We sampled each vector with an averaging period window of 1.0 s and a 500 ms delay to attenuate vibrations on the robot. The total exploration lasted approximately 70 s. A binarizing threshold of lth $= 0.1\frac{m}{s^2}$, which is 10% of the maximum change of $1.0\frac{m}{s^2}$, proved to be sufficiently sensitive and robust against sensor noise and balancing motions of the robot. With the HRP-2, we only performed one (position) incremental run, followed by one decremental run on all DoFs, combining entries from both ($P = 2$) postural runs with an element wise 'or'. In this case, the simplified approach worked because the first DoF of each arm is not aligned with the gravity vector. If this was not the case, we only need to change the posture of the robot to avoid this singular condition. We could not detect any error in the kinematic tree with all ($N \geq 10$) runs (see Figure 10).

4.3. Sensory-motor mapping

The sensory-motor map is a set of postural matrices, mapping distributed tactile stimulations into joint-level robot reactions, grounded on the reference body part, e.g. the torso of a humanoid. In this context, it is a kind of Jacobian-based inverse kinematic solution for numerous distributed contact points on the surface of the robot. The map is acquired automatically and replaces manual calibration efforts for the robot kinematics, as well as the placement/orientation of skin sensors on its surface.

4.3.1. Exploration pattern

In order to evaluate the influence of each revolute DoF (d), on the translational motion of a sensor cell (s), in a pose (p), the robot applies test pattern to one DoF after the other. Due to the currently available tactile sensors, i.e. normal force and proximity, we here focus on the translational component in direction of the surface normal. For the translational components, only the tangential acceleration ${}^u\vec{a}_{u,d}^{\tan}$ can be utilized, as it is collinear with the local motion vector. The influence of the centripetal acceleration can be minimized by keeping the angular velocity ω_d low. The influenced of the rotated gravity vector is nearly constant, and thus subtractable, when the DoF motion only covers a small angular range $\triangle\varphi_d$. In order to maximize the tangential acceleration, the angular acceleration α_d has to be high. In order to maintain smooth accelerometer readings, it is necessary to control the angular velocity $\omega_d(t)$, the acceleration $\alpha_d(t)$, and the jerk $\zeta_d(t)$. It is desirable that the DoF returns to its initial position $\varphi_d(0) = \varphi_d(T)$ once the exploration pattern stops at time T. One velocity control pattern $\omega_d(t)$ that fulfills all requirement is a sine wave:

$$\varphi_d(t) = \frac{A}{2\pi f}(1 - \cos(2\pi f t)) \quad \text{(position)} \tag{5}$$

$$\omega_d(t) = A\sin(2\pi f t) \quad \text{(velocity)} \tag{6}$$

$$\alpha_d(t) = 2\pi f A \cos(2\pi f t) \quad \text{(acceleration)} \tag{7}$$
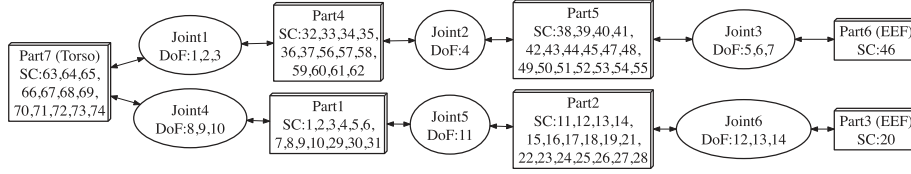
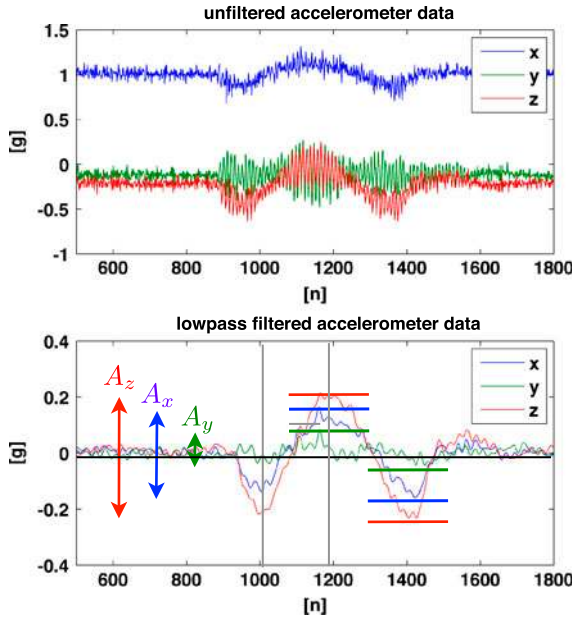Figure 10. Structural exploration result for the kinematic tree of HRP-2's upper body.

Figure 11. Sensory motor map weight extraction from raw accelerometer data.

$$\zeta_d(t) = -(2\pi f)^2 A \sin(2\pi f t) \quad \text{(jerk)} \quad (8)$$

These equations help us to dimension the DoF exploration pattern. The selection of A is limited by the maximum DoF velocity and the tolerable influence of the centripetal acceleration. $2\pi f A$ has to be lower than the maximum DoF acceleration and below a value that shows undesired dynamic side effects. $\frac{A}{2\pi f}$ has to be small enough to be able to neglect the influence of the rotating gravity vector and the postural change of the robot. Still $2\pi f A$, has to be sufficiently large that the measurement of the accelerometer $^u\vec{a}_{u,d}$ of sensor cell (u) stands out from its intrinsic sensor noise. A windowing function $W(t)$ is necessary to cut the executed pattern in time $\omega_d^{ex}(t)$ and stop the robot in its initial posture:

$$\omega_d^{ex}(t) = W(t) \cdot \omega_d(t) \quad (9)$$

We currently utilize a rectangular function, cutting the oscillation after one period ($T = \frac{1}{f}$). Commonly, we make use of the same empirical values across different robots: $A = 0.4\frac{\text{rad}}{\text{s}}$, $f = 2\,\text{Hz}$ and $T = 0.5\,\text{s}$, e.g. tested on UR-5, HRP-2 or the KUKA LWR.

4.3.2. Pattern evaluation

A distinct value quantifies the contribution of a DoF (d), towards the desired motion of a sensor cell (u) in the current pose (p). We first subtract the mean value from all accelerometer axes, in order to eliminate constant sensor offsets and the gravity vector $^u\vec{g}$. We then apply a digital low-pass filter, with a bandwidth B larger than 10 times the pattern frequency f, to eliminate noise and vibrations. Finding the minimum and maximum, we then calculate the amplitude for every axis (see Figure 11), here along the z-axis $^u\vec{e}^z$ of the accelerometer $A_{u,d,p}^z$:

$$A_{u,d,p}^z = \max(^u a_{u,d}^z) - \min(^u a_{u,d}^z) \quad (10)$$

In order to discriminate if the desired motion is in-phase or anti-phase, we evaluate if the minimum or maximum is located first in time (MATLAB terminology):

$$s_{u,d,p}^z = \text{sign}\left(\text{find}\left(^u a_{u,d}^z == \max(^u a_{u,d}^z), \text{`first'}\right)\right.$$
$$\left. -\text{find}\left(^u a_{u,d}^z == \min(^u a_{u,d}^z), \text{`first'}\right)\right) \quad (11)$$

The weight $w_{u,d,p}^z$, in the local sensor cell surface normal direction $^u\vec{e}^z$, is now computed as:

$$w_{u,d,p}^z = s_{u,d,p}^z \cdot \frac{A_{u,d,p}^z}{A_{u,d,p}^x + A_{u,d,p}^y + A_{u,d,p}^z} \quad (12)$$

Weights can thus have values between $[-1; 1]$, being close to ± 1 if the DoF motion fully correlates with the desired translational motion, while being close to 0 in the orthogonal cases.

4.3.3. Sensory-motor map

The sensory motor map is a container for the explored weight values, acting as a lookup table for the mapping of tactile reactions. Each tile of the sensory motor map is explored in a pose (p), and features up to three sets of matrices, related to the three translational directions. The dimension of each matrix is defined by the available sensor cells and degrees of freedom ($U \times D$). Due to our current set of sensor modalities, we only make use of the matrix values $w_{u,d,p}^z$ collinear to the surface normal. Each tile also contains a vector of the robot pose it has been explored in. This helps to recall the closest (e.g. quadratic distance) memorized pose when mapping tactile reactions
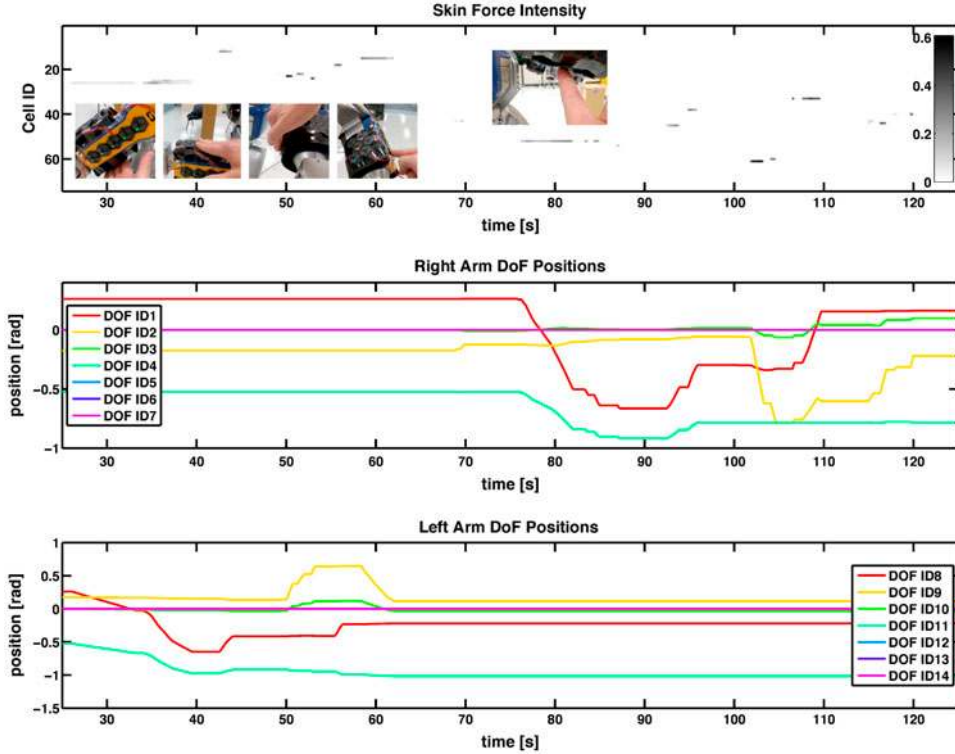
Figure 12. Tactile guidance with the normal force sensors – Stimulations are directly mapped to evasive motor reactions via the sensory-motor map.

Table 3. Heuristic normalized tactile event levels.

Force cells		Pre-contact sensor	
Pain force		Close contact	
	0.45		0.80
High force		Low proximity	
	0.30		0.10
Medium force		Medium proximity	
	0.10		0.02
Low force		High proximity	
	0.04		0.01
No force		No proximity	

into robot reactions. On robots with multiple kinematic chains, e.g. a humanoid with two arms, dynamic coupling effects in between moving body parts are likely. In this case, a post-processing of the postural matrices with the structural knowledge helps to decouple those body parts. Here, we element wise multiply ($\circ$) the global activity matrix (AM) with each sensory motor map matrix (W_p):

$$W_{p,\text{new}} = \text{AM} \circ W_p \qquad (13)$$

Additionally, small sensor cell reaction vectors ($\vec{w}_{u,p}^{z}$) must be cut, as those reactions cannot be grounded on a static reference like the torso, but require e.g. locomotion. Vectors above this suppression threshold must be normalized to bal-

ance the tactile reaction strength along the entire kinematic chain.

5. Controlling multi-modal, whole-body tactile interaction

5.1. Multi-modal, cellular reaction primitives

The sense of touch allows to implement meaningful direct reactions on multi-modal tactile stimulation – e.g. to avoid self- or environment collisions or to let users kinesthetically guide the robot. The advantage of instantiating one multi-modal reaction controller for every sensor cell (u) is the scalability of this approach – tactile behavior can be

programmed for the smallest piece of skin and expanded to the whole robot surface. Since all cellular parameters, are accessible by the high-level control system, spatial reactions can be set up for a specific task. In this paper, we compute a proportional motor reaction for every multi-modal (m) sensor value (ρ_m) above a pre-defined threshold (t_m). All (M) multi-modal reactions on a cell are then accumulated and mapped to a desired cellular velocity reaction vector, via the sensory-motor map. Super-imposing the resulting velocity vectors from all (U) sensor cells, leads to a global tactile robot joint velocity reaction ($\vec{\omega}_{\text{tactile}}$):

$$\vec{\omega}_{\text{tactile}} = \sum_{u=1}^{U} \left(\vec{w}_{u,p} \cdot \sum_{m=1}^{M} (\rho_m > t_m) \cdot (\rho_m - t_m) \cdot P_m \right)$$
(14)

Modalities can be inhibited, promoted or inverted by setting their gain ($P_{m,u}$). The threshold ($t_{m,u}$) determines the activation level and is important to suppress sensor noise and offsets. We, commonly, directly act on persistent sensor data (e.g. force or proximity), omitting additional reaction delays and computational efforts. In case smoother reactions are desired, either the stimuli or the executed response can be extended/filtered in time, damping the whole system. With time singular tactile stimulations, e.g. the detection of impacts via vibrational cues like in [27], a temporal response is inevitable.

5.2. Cellular tactile events

Centrally monitoring a growing number of tactile sensors, generates high computational and network overloads. Since most skin areas are not (or in constant) contact, this effort is commonly in vain. To prevent this scalability bottleneck, we pre-process tactile signals into events. Currently, this is still done on the computer, as we wish to log all raw experimental data. But by design, CellulARSkin allows to locally process tactile signals in every sensor cell, extracting information at the earliest stage. New data packets should only be generated if sensor values deviate significantly from sensor noise and recently transmitted samples. Therefore, all our high-level algorithms make use of abstract tactile events, while our low-level control algorithms can deal with varying update rates. For our grasping approach on HRP-2, we utilized force and proximity events, with a coarse separation into heuristically pre-defined levels (refer to Table 3). A new tactile event is only emitted on changes between those levels, with a small hysteresis to prevent repetitive triggers. Due to the direct localization of touch, tactile events in specific areas can trigger robot behaviors or state changes, e.g. launch a grasping sequence when patted on the shoulder.

5.3. Experiments on HRP-2

The effectiveness of tactile reactions, and their transfer to motor actions through the sensory-motor map on a hum-

anoid robot, can be best evaluated on kinesthetic tactile guidance. We currently provide two different modes: (i) force guidance; and (ii) proximity guidance. Force guidance takes the force modality into account and thus requires physical contact with the robot. With the pre-contact sensor, and thus proximity guidance, the robot will start to react before the user touches the robot (here ∼5 cm before). In Figure 12, we show a plot of force guidance with both arms, first left then right. The activation threshold (t_m) of 0.05 raw force cell readings (ρ_m), approximately relates to 0.6 N, the chosen force gain (P_m) is 1.0 (see Equation 14). A single-force cell reading of $\rho_{F1} = 0.14$, relating to a force of 1.0 N, is transferred to a commanded velocity of $\vec{\omega}_{re} = 0.09$rad/s on a single DoF – which is approximately what can be seen between 75 s and 85 s with actuator ID1 (neglecting ID4 and 2) and sensor cell ID52. All key poses for the grasping application have been taught via the pre-contact sensor, enabling the most pleasant user experience.

6. Application of whole-body tactile interaction

6.1. Grasping approach

Our whole-body grasping approach has been inspired by observing human. Human commonly pull large and unknown objects with both arms to the chest. This approach is very effective, as three distal contact points define a stable grasp, large and compliant contact areas (CA) distribute applied forces and provide shear stability, the potentially large weight is close to the center of mass and short kinematic chains reduce the required joint forces. In order to quickly replicate this human behavior with our artificial skin system on HRP-2, we had to (1) teach the robot grasping and pulling trajectories for both arms; (2) define areas to make contact with and allow forces to be applied within; (3) coordinate the grasping sequence with a tactile event driven state machine; and (4) use tactile reactions to adapt grasping trajectories to the size and stiffness of the object.

6.2. Grasping trajectories

We utilized kinesthetic teaching to interactively drive the robot to different key poses (see Figure 13). Interpolations between those key poses were then utilized to generate the grasping trajectories. The robot starts from the safe 'home' key pose. In the 'open' key pose, both arms are opened widely to make space for an object in between. The 'closed' key pose brings both arms together so an object in between is inevitably made contact with. In the 'pulled' key pose, both arms are still together, but the arms are pulled closer to the chest, so any object between the arms must come into contact with the chest. All key poses are added to the sensory-motor map, in order to correctly map tactile reactions around them. The trajectory generator calculates velocity commands to transition the robot in joint space from the current pose ($\vec{\varphi}_{\text{cur}}$) to a desired ($\vec{\varphi}_{\text{des}}$) key
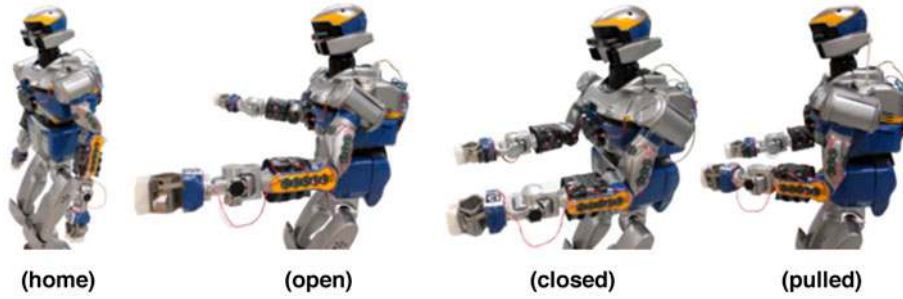
Figure 13. Grasping trajectory key poses, taught to the robot via tactile guidance.
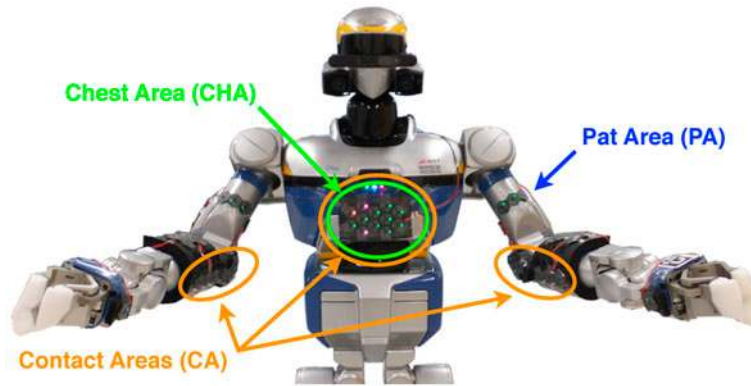

Figure 14. Touch areas: allocated with specific reactions and monitoring specific events.
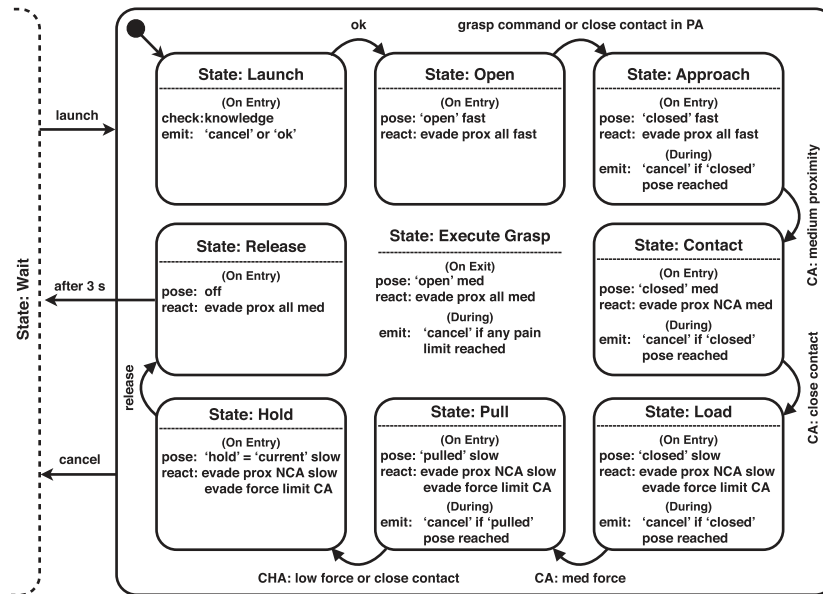

Figure 15. State-machine of the grasping sequence: triggered by tactile events, controlling the trajectory generation between key poses and coordinating the whole-body tactile reaction primitives.

pose. Control parameters define the maximum joint velocity ($\omega_{\max}$), the desired postural accuracy (φ_{acc}), the name of the pose and a flag if the robot should stop once the desired

key pose has been reached. On reaching a desired pose, an event is sent to the control system. For the overall reaction of the robot, the tactile reaction velocity vector ($\vec{\omega}_{\mathrm{tactile}}$) and
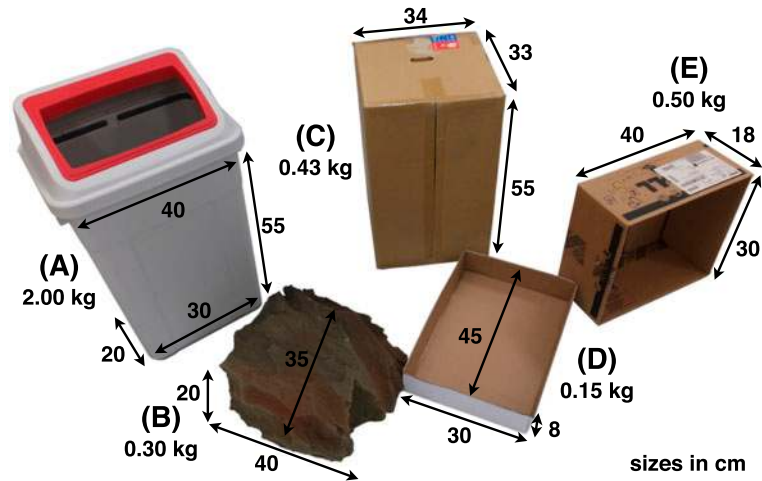
Figure 16. Objects utilized to test the graping approach: (A) plastic trash bin; (B) sponge rock; (C) moving box; (D) lid of a paper box; and (E) computer delivery box. The objects have different weights, shape, hardness, and size.

Figure 17. A position controlled HRP-2 humanoid, holding unknown objects with the whole-body, as result of a multi-modal tactile grasping sequence.

Table 4. Heuristic control parameters of the grasping experiment.

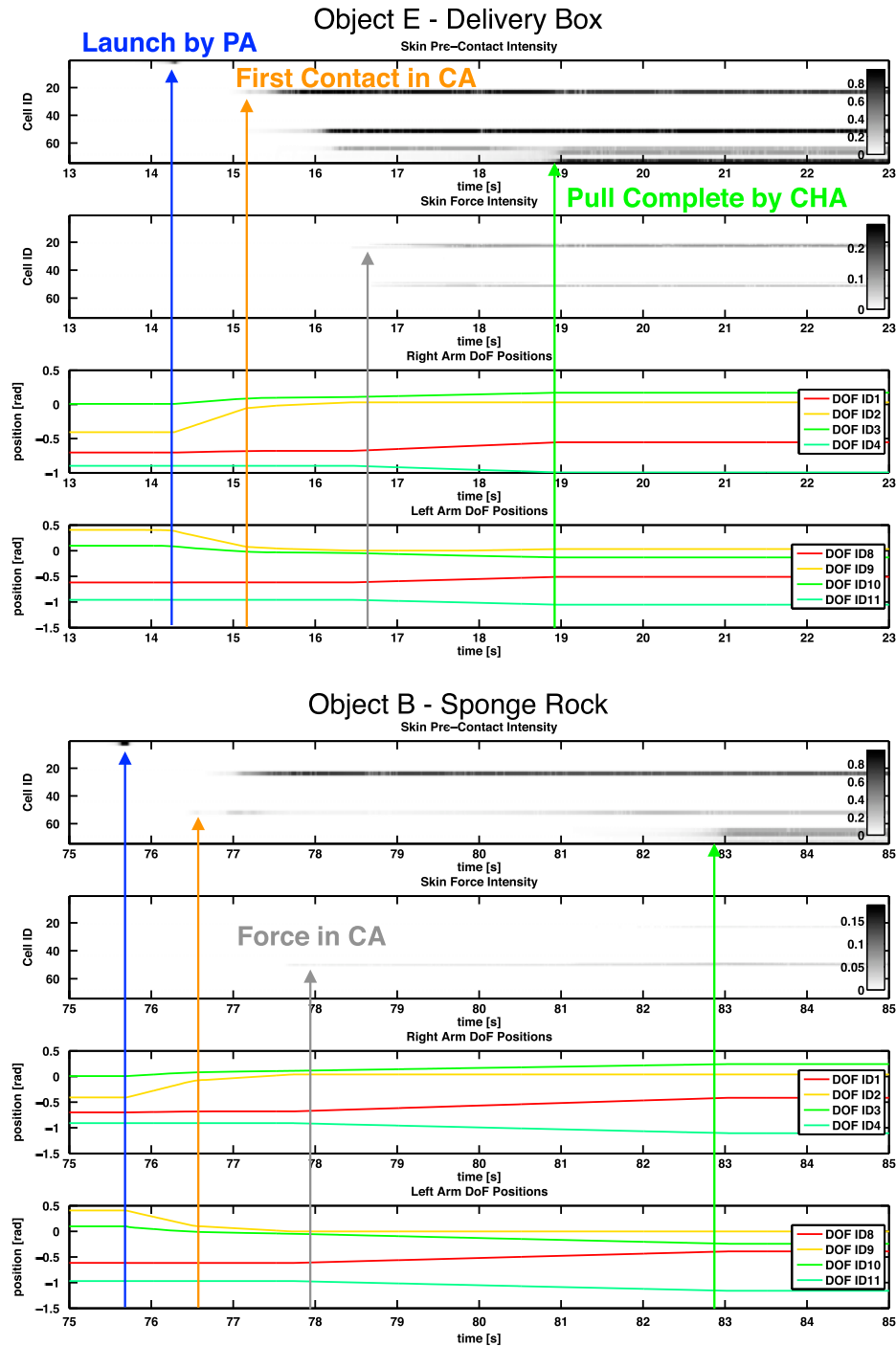| State	Force		Pre-contact		Pose		
	t_F	P_F	t_P	P_P	Hash	ω_{max}	φ_{acc}
F-guide	0.05	1.0	–	0.0	–	–	–
Open	–	0.0	0.01	0.4	Open	0.4	0.01
Approach	–	0.0	0.01	0.4	Closed	0.4	0.01
Contact	–	0.0	–N 0.01 C	0.0 N 0.4 C	Closed	0.1	0.01
Load	–N –C	0.00 N 0.00 C	0.01 N –C	0.01 N 0.00 C	Closed	0.05	0.01
Pull	–N 0.10 C	0.00 N 0.80 C	0.01 N –C	0.01 N 0.00 C	Pulled	0.05	0.01
Hold	–N 0.10 C	0.00 N 0.80 C	0.01 N – C	0.01 N 0.00 C	–	–	–
Release	–	0.0	0.01	0.2	–	–	–

Figure 18. Proprioceptive and tactile feedback while grasping two objects (E/B) with different compliance (hard/soft) and shape (regular/irregular).

trajectory velocity vector ($\vec{\omega}_{\text{traject}}$) are super-imposed. Which is why tactile reactions have to be dominant in comparison to the trajectory speed and/or cancel the current trajectory execution in case of detected 'pain' levels.

6.3.　Touch areas

For our grasping approach, we defined three different types of touch areas (see Figure 14). Every touch area is assigned with different reaction primitives and event monitors. The

'pat' area acts as a kind of launch or emergency button, a contact in this area starts or terminates the grasping sequence and triggers the release of an object. The CA are parts of the surface, the robot is supposed to contact and hold the object with. The CA allow touch, while multi-modal events, in this areas, determine if the 'approach' or 'load' state have been completed. The chest area serves as a third explicit contact point. A close contact in this area completes the grasping sequence. Remaining sensor cells are automatically allocated to the non-contact areas (NCA). Contacts in these areas are avoided to prevent self- or environment collisions.

6.4. Grasp state machine

The whole grasping sequence is split into multiple states of a sequential state machine (see Figure 15). As an entry action, every state sends a set of area specific control directives to the low-level tactile controllers. Changes between states are triggered by events from the trajectory generator or tactile events. Emergency situations, e.g. pain level forces, drive the robot into a safe state. The safest action is not to stop all upper body motions (lesson learned with two burnt motors), but to slowly evade all contacts. States with contact as main objective (e.g. the approach, contact, load, or pull state), fail if the set key pose can be reached prior to satisfactory tactile interaction. In the 'approach' state, the object needs to come close to the expected CA, while forces have to be applicable in the 'load' state. In general, the interaction speed is reduced the closer the robot and object come together. Here, we specifically make use of the pre-contact modality to safely increase the speed in the approach and contact phase (refer to Table 4). Purely relying on the force sensors, forces could ramp up quicker than the reaction time of the robot, damaging the robot or the object. With HRP-2 and CellulARSkin we solved this issue by: (i) using the on-board computer to minimize delays; (ii) adding a foam layer between the robot and the skin to provide (sensor) hysteresis free compliance; and (iii) using pre-contact sensors to slow down motion before contact.

6.5. Experiments on HRP-2

In Figure 16, we show a set of five objects with different weight, size, shape, and compliance, which we successfully tested our approach on (see Figure 17). We applied the same set of heuristic control parameters for all objects (refer to Table 4). A grasp succeeded, when the robot was able to make contact with the object, apply forces on it and pull it to the chest. Our approach infers that the graspable object is in between both arms when receiving the launch command. If there is no object, or the object cannot be pulled, the robot automatically cancels the grasp. The plastic cover on the wrist does not support force and is such allocated to the NCA, where applied forces intentionally cancel the grasp.

Naturally, this limits our success rate when grasping big objects, like the trash bin or the big moving box, as big objects are likely to touch the wrist. We wish to emphasize that no object has been damaged during all experiments. To demonstrate our trust in the system, we let the robot 'hug' human multiple times (first author). The pre-contact modality allows to speed up motions prior to contact and robustly detects when the object touches the chest, which is sufficient to prevent the rotation of grasped objects. The advantages of our multi-modal approach, triggering and controlling phases of the grasping approach with different sensor modalities, can be seen in Figure 18. As a consequence of the similar size, both objects (B and E) are first contacted after nearly the same time. First light contact forces also build up in a similar time frame. However, it is already visible in the pre-contact intensity, that object E has a symmetric surface, while object B is asymmetric. This observation continues within the force profile, where object E develops and maintains a clear and symmetric contact force intensity on both arms, while object B remains squishy. Due to the conformation of object B to the robot's surface, and the incomplete coverage with skin, forces for object B are in parts grounded on insensitive spots, which is visible in the remaining sensational asymmetry. Both grasps are finalized with a close contact on the chest, but after a significantly different time span. This can be explained, as Object B had to be pulled over a longer distance and compressed for a longer time to maintain 'satisfying' contact pressure.

6.6. Media attachment

We would also like to direct the interested reader to our attached video. The video introduces a quick overview of all implemented self-exploration steps, the teach-in process, and shows exemplary object grasps.

7. Conclusion

For the first time, we applied our multi-modal artificial skin, and its self-organizing features, on a full-sized humanoid robot. We explained novel approaches to automatically acquire kinematic knowledge, for a new type of cellular tactile control algorithms. In comparison to existing approaches, our grasping algorithm requires little knowledge on the robot it controls (no kinematic/dynamic model) and the object it handles (no object model). Utilizing pre-contact sensors for a novel way of teaching behaviors, it is not necessary to apply force on the robot or even touch it – making heavy or position controlled robots featherlight to interact with. Relying only on artificial skin, no joint-level force sensing is required.

Acknowledgements

Tsukuba, Japan and by the DFG cluster of excellence Cognition for Technical systems – CoTeSys. Many thanks to Thomas Moulard and Pierre Gergondet, for helping with the robot HRP-2, and the whole CNRS/AIST team.

Supplemental data

Supplemental data for this article can be accessed at http://dx.doi.org/10.1080/01691864.2014.952493.

Notes on contributors

Philipp Mittendorfer received his bachelors degree in electrical engineering from Technische Universität München, Munich, Germany, in 2008, and the Diploma degree in 2009. Since December 2009, he has been with the Tactile Sensing Group with Gordon Cheng, Institute for Cognitive Systems, Technische Universität München. His current research interests include methods to self-organize intelligent surface sensor networks and their practical implementation as multi-modal artificial sensor skins into robotic systems.

Eiichi Yoshida received ME and PhD degrees on Precision Machinery Engineering from Graduate School of Engineering, the University of Tokyo in 1993 and 1996, respectively. From 1990 to 1991, he was visiting research associate at Swiss Federal Institute of Technology at Lausanne (EPFL). In 1996, he joined former Mechanical Engineering Laboratory, later reorganized as National Institute of Advanced Industrial Science and Technology (AIST), Tsukuba, Japan. He served as co-director of AIST/IS-CNRS/ST2I Joint French-Japanese Robotics Laboratory (JRL) at LAAS-CNRS, Toulouse, France, from 2004 to 2008. Since 2009, he is co-director of CNRS-AIST JRL (Joint Robotics Laboratory), UMI3218/CRT, Tsukuba, Japan. His research interests include robot task and motion planning, modular robotic systems, and humanoid robots.

Gordon Cheng is the professor and chair of Cognitive Systems, and founding director of the Institute for Cognitive Systems, Technische Universität München, Munich, Germany. He was the head of the Department of Humanoid Robotics and Computational Neuroscience, ATR Computational Neuroscience Laboratories, Kyoto, Japan, from 2002 to 2008. He was the group leader for the JST International Cooperative Research Project, Computational Brain, from 2004 to 2008. He was designated a project leader from 2007 to 2008 for the National Institute of Information and Communications Technology of Japan. He has held visiting professorships worldwide in multidisciplinary fields comprising mechatronics in France, neuroengineering in Brazil, and computer science in the USA. He held fellowships from the Center of Excellence and the Science and Technology Agency of Japan. Both of these fellowships were taken at the Humanoid Interaction Laboratory, Intelligent Systems Division at the Electrotechnical Laboratory, Japan. He received PhD degree in systems engineering from the Department of Systems Engineering, The Australian National University, in 2001, and the bachelors and masters degrees in computer science from the University of Wollongong, Wollongong, Australia, in 1991 and 1993, respectively. He was the managing director of the company G.T.I. Computing in Australia. His current research interests include humanoid robotics, cognitive systems, brain machine interfaces, biomimetic of human vision, human-robot interaction, active vision, and mobile robot navigation. He is the co-inventor of approximately 15 patents and has co-authored approximately 180 technical publications, proceedings, editorials, and book chapters.

References

[1] Harmon LD. Automated tactile sensing. Int. J. Robot. Res. 1982;1:3–31.

[2] Dahiya RS, Mittendorfer P, Valle M, Cheng G, Lumelsky VJ. Directions toward effective utilization of tactile skin: a review. IEEE Sensor. J. 2013;13:4121–4138.

[3] Someya T, Sekitani T, Iba S, Kato Y, Kawaguchi H, Sakurai T. A large-area, flexible pressure sensor matrix with organic field-effect transistors for artificial skin applications. Proc. Nat. Acad. Sci. USA. 2004;101:9966–9970.

[4] Dahiya RS, Metta G, Valle M, Sandini G. Tactile sensing-from humans to humanoids. IEEE Trans. Robot. 2010;26:1–20.

[5] Alirezaei H, Nagakubo A, Kuniyoshi Y. A tactile distribution sensor which enables stable measurements under high and dynamic stretch. In: IEEE Symposium on 3D User Interfaces; 2009; Lafayette, LA, USA. p. 87–93.

[6] Hakozaki M, Hatori A. A sensitive skin using wireless tactile sensing elements. In: Technical Digest of the 18th Sensor Symposium; 2001; Kawasaki, Japan. Vol. 18. p. 147–150.

[7] Strohmayr M. Artificial skin in robotics [PhD thesis]. Karlsruhe, Germany: Karlsruher Institut fuer Technologie; 2012.

[8] Hoshi T, Shinoda H. A tactile sensing element for a whole body robot skin. In: Proceedings on the 36th International Symposium on Robotics; 2005; Tokyo, Japan.

[9] Cannata G, Maggiali M, Metta G, Sandini G. An embedded artificial skin for humanoid robots. In: Proceedings of IEEE International Conference on Multisensor Fusion and Integration for Intelligent Systems; 2008; Seoul, South Korea. p. 434–438.

[10] Goeger D, Weiss K, Burghart C, Woern H. Sensitive skin for a humanoid robot. In: International Workshop on Human-Centered Robotic Systems; 2006; Munich, Germany.

[11] Ohmura Y, Kuniyoshi Y, Nagakubo A. Conformable and scalable tactile sensor skin for curved surfaces. In: International Conference on Robotics and Automation; 2006; Orlando, FL, USA. p. 1348–1353.

[12] Iwata H, Sugano S. Design of human symbiotic robot twendy-one. In: International Conference on Robotics and Automation; 2009; Kobe, Japan. p. 580–586.

[13] Cannata G, Denei S, Mastrogiovanni F. On internal models for representing tactile information. In: IEEE International Conference on Intelligent Robots and Systems; 2010; Taipei, Taiwan. p. 1108–1113.

[14] Kuniyoshi Y, Yorozu Y, Ohmura Y, Terada K, Otani T, Nagakubo A, Yamamoto T. From humanoid embodiment to theory of mind. Lect. Notes Comput. Sci. 2004;3139:202–218.

[15] Hoffmann M, Marques HG, Arieta AH, Sumioka H, Lungarella M, Pfeifer R. Body schema in robotics: a review. IEEE Trans. Auton. Ment. Dev. 2010;2:304–324.

[16] Fuke S, Ogino M, Asada M. Body image constructed from motor and tactile images with visual information. Int. J. Humanoid Rob. 2007;4:347–364.

[17] Prete AD, Denei S, Natale L, Mastrogiovanni F, Nori F, Cannata G. Skin spatial calibration using force/torque measurements. In: IEEE/RSJ International Conference on Intelligent Robots and Systems; 2011; San Francisco, CA, USA. p. 3694–3700.

[18] Yoshikawa Y, Kawanishi H, Asada M, Hosoda K. Body scheme acquisition by cross modal map learning among tactile, visual, and proprioceptive spaces. In: Proceedings of the Second International Workshop on Epigenetic Robotics; 2002; Edinburgh, Scotland, UK.

[19] Olsson L, Nehaniv CL, Polani D. From unknown sensors and actuators to actions grounded in sensorimotor perceptions. Connection Sci. 2006;18:121–144.

[20] Cannata G, Denei S, Mastrogiovanni F. Contact based robot control through tactile maps. In: 49th IEEE Conference on Decision and Control (CDC); Atlanta, GA, USA. p. 3578–3583.

[21] Romano JM, Hsiao K, Niemeyer G, Chitta S, Kuchenbecker KJ. Human-inspired robotic grasp control with tactile sensing. IEEE Trans. Rob. 2011;27:1067–1079.

[22] Mukai T, Onishi M, Odashima T, Hirano S, Luo Z. Development of the tactile sensor system of a human-interactive robot ri-man. IEEE Trans. Rob. 2008;24:505–512.

[23] Mukai T, Hirano S, Yoshida M, Nakashima H, Guo S, Hayakawa Y. Whole-body contact manipulation using tactile information for the nursing-care assistant robot riba. In: International Conference on Intelligent Robots and Systems; 2011; San Francisco, CA, USA. p. 2445–2451.

[24] Ohmura Y, Kuniyoshi Y. Humanoid robot which can lift a 30kg box by whole body contact and tactile feedback. In: International Conference on Intelligent Robots and Systems; 2007; San Diego, CA. p. 1136–1141.

[25] Kumagai l, Kobayashi K, Nozawa S, Kakiuchi Y, Yoshikai T, Okada K, lnaba M. Development of a full body multi-axis soft tactile sensor suit for life sized humanoid robot and an algorithm to detect contact states. In: IEEE International Conference on Humanoid Robots; 2012; Osaka, Japan. p. 526–531.

[26] Mittendorfer P, Cheng G. Integrating discrete force cells into multi-modal artificial skin. In: IEEE International Conference on Humanoid Robots; 2012; Osaka, Japan. p. 847–852.

[27] Mittendorfer P, Cheng G. Humanoid multi-modal tactile sensing modules. IEEE Trans. Rob. 2011;27:401–410.

[28] Mittendorfer P, Cheng G. Open-loop self-calibration of articulated robots with artificial skins. In: IEEE International Conference on Robotics and Automation; 2012; Saint Paul, MN, USA. p. 4539–4545.

[29] Mittendorfer P. Self-organizing sensory-motor map for low-level touch reactions. In: 11th IEEE-RAS International Conference on Humanoid Robots; 2011; Bled, Slovenia. p. 59–66.

[30] Kaneko K, Kanehiro F, Kajita S, Hirukawa H, Kawasaki T, Hirata M, Akachi K, Isozumi T. Humanoid robot hrp-2. In: IEEE International Conference on Robotics and Automation; 2004; Barcelona, Spain. p. 1083–1090.

[31] Mansard N, Stasse O, Evrard P, Kheddar A. A versatile generalized inverted kinematics implementation for collaborative humanoid robots: the stack of tasks. In: International Conference on Advanced Robotics; 2009; Munich, Germany. p. 1–6.

[32] Mittendorfer P, Yoshida E, Moulard T, Cheng G. A general tactile approach for grasping unknown objects with a humanoid robot. In: IEEE International Conference on Intelligent Robots and Systems; 2013; Tokyo, Japan. p. 4747–4752.

[33] Park J-J, Haddadin S, Song J-B, Albu-Schaeffer A. Designing optimally safe robot surface properties for minimizing the stress characteristics of human-robot collisions. In: IEEE International Conference on Robotics and Automation; 2011; Shanghai, China. p. 5413–5420.